Science and Technology of Advanced Materials

ISSN: (Print) (Online) Journal homepage: www.tandfonline.com/journals/tsta20

Alkyl anchor–modified artificial viral capsid budding outside-to-inside and inside-to-outside giant vesicles

Kazunori Matsuura, Miu Hirahara, Kentarou Sakamoto & Hiroshi Inaba

To cite this article: Kazunori Matsuura, Miu Hirahara, Kentarou Sakamoto & Hiroshi Inaba (29 Apr 2024): Alkyl anchor–modified artificial viral capsid budding outside-to-inside and inside-to-outside giant vesicles, Science and Technology of Advanced Materials, DOI: 10.1080/14686996.2024.2347191

To link to this article: https://doi.org/10.1080/14686996.2024.2347191

Publisher: Taylor & Francis & The Author(s). Published by National Institute for Materials Science in partnership with Taylor & Francis Group.

Journal: *Science and Technology of Advanced Materials*

DOI: 10.1080/14686996.2024.2347191

Alkyl anchor–modified artificial viral capsid budding outside-to-inside and inside-to-outside giant vesicles

Kazunori Matsuura[a,b], Miu Hirahara[a], Kentarou Sakamoto[a], Hiroshi Inaba[a,b]

[a] *Department of Chemistry and Biotechnology, Graduate School of Engineering, Tottori University, Tottori, Japan*

[b] *Center for Research on Green Sustainable Chemistry, Tottori University, Tottori, Japan*

CONTACT: Kazunori Matsuura, ma2ra-k@tottori-u.ac.jp, Department of Chemistry and Biotechnology, Graduate School of Engineering, Tottori University, 4–101 Koyama-Minami, Tottori 680-8552, Japan

Alkyl anchor–modified artificial viral capsid budding outside-to-inside and inside-to-outside giant vesicles

The budding of human immunodeficiency virus from an infected host cell is induced by the modification of structural proteins bearing long-chain fatty acids, followed by their anchoring to the cell membrane. Although many model budding systems using giant unilamellar vesicles (GUVs) induced by various stimuli have been developed, constructing an artificial viral budding system of GUVs using only synthesized molecules remains challenging. Herein, we report the construction of an artificial viral capsid budding system from a lipid bilayer of GUV. The C-terminus of the β-annulus peptide was modified using an octyl chain as an alkyl anchor via a disulfide bond. The self-assembly of the β-annulus peptide with an octyl chain formed an artificial viral capsid aggregate. The fluorescence imaging and transmission electron microscopy observations revealed that the addition of the tetramethylrhodamine (TMR)-labeled octyl chain–bearing β-annulus peptide to the outer aqueous phase of GUV induced the budding of the capsid-encapsulated daughter vesicle outside-to-inside the mother GUV. Conversely, the encapsulation of the TMR-labeled octyl chain–bearing β-annulus peptide in the inner aqueous phase of GUV induced the budding of the capsid-encapsulated daughter vesicle inside-to-outside the mother GUV. Contrarily, the addition of the TMR-labeled β-annulus peptide to GUV barely induced budding. It was demonstrated that the higher the membrane fluidity of GUV, the more likely budding would be induced by the addition of the alkyl anchor–modified artificial viral capsid. The simple virus-mimicking material developed in this study, which buds off through membrane anchoring, can provide physicochemical insights into the mechanisms of natural viral budding from cells.

Keywords: artificial viral capsid; self-assembly; β-annulus peptide; alkyl anchor; budding; giant vesicle

1. Introduction

Natural nonenveloped viruses are discrete nanostructures comprising nucleic acids encapsulated in self-assembled capsid proteins, whereas enveloped viruses are complexes exhibiting a nucleocapsid structure surrounded by a lipid bilayer embedding

membrane proteins. Natural viruses can self-replicate by hijacking biosynthetic systems within an infected host cell, followed by budding out of the cell membrane, to infect the next host cell [1]. Viral capsid proteins self-assemble around the cell membrane by anchoring various signaling proteins to the membrane, and the virus is enveloped by the cell membrane and released outside the cell. For example, the nucleocapsid of human immunodeficiency virus type 1 (HIV-1) buds out of the infected cell by binding and localizing to the plasma membrane through the myristoylation of the N-terminal matrix domain of the viral structural protein Gag [2-4]. Influenza viruses undergo budding through changes in their membrane curvature triggered by the interactions between the matrix proteins on the plasma membrane and membrane proteins, such as hemagglutinin and neuraminidase [5].

Studies have demonstrated that experimental model systems using giant unilamellar vesicles (GUVs) improve the physicochemical understanding of cell division and cells [6]. To date, the budding, division, and deformation of GUVs induced by the osmotic shrinkage of aqueous two-phase systems [7-9], pore-forming peptides [10], phospholipid production [11], sphingomyelin degradation [12], thermoresponsive polymers [13], membrane-bound proteins [14], and cholesterol-modified four-branch deoxyribonucleic acids (DNA) [15] have been reported. A minimal biomimetic budding system was constructed by adding the HIV-1 Gag protein and urea to GUV [16]. However, the construction of an artificial budding system for viruses from GUVs using only synthesized molecules remains challenging. Constructing such an artificial viral budding system will improve the physicochemical understanding of natural viral budding and facilitate the development of artificial molecular transport systems between cells or GUVs.

The self-assembly of rationally designed peptides facilitates the construction of viral capsid-like nanocapsules [17]. We previously constructed an artificial viral capsid by self-assembling 24-residue *β*-annulus peptides (INHVGGTGGAIMAPVAVTRQLVGS) involved in the formation of the dodecahedral internal skeleton of the tomato bushy stunt virus [18]. The C-terminus of the *β*-annulus peptide is directed to the outer surface, whereas the N-terminus is directed to the interior of the artificial capsids [19]. Further, the N-terminal modification enabled the encapsulation of guest macromolecules, whereas the C-terminal modification enabled the display of various functional molecules, such as proteins and DNAs, on the outer surface [17, 19-27]. Recently, we demonstrated the construction of an enveloped artificial viral capsid by the complexation of an anionic artificial viral capsid (self-assembled from β-annulus-EE peptide) with a cationic lipid bilayer through electrostatic interaction [28-31].

One strategy for transporting and localizing molecules onto the lipid bilayer is subjecting the molecule to alkyl anchoring modification [32-35]. By mimicking the budding mechanism of HIV-1 by the myristoyl modification of Gag protein [2-4], modifications that ensure the transport of artificial viral capsids to the lipid bilayer and enable the construction of an artificial viral budding system can be achieved. Artificial virus capsids that can be appropriately dispersed in water without considerable aggregation and appropriately anchored on GUV membranes must be developed. Thus, to construct an alkyl anchor–modified artificial viral capsid, we designed a β-annulus peptide bearing an octyl chain exhibiting moderate hydrophobicity via a disulfide bond at the C-terminus directed toward the outer surface of the capsid (Figure 1). In this study, we demonstrated that the octyl chain–bearing β-annulus peptide induces budding outside-to-inside and inside-to-outside GUVs. In addition, we proposed a method for

constructing enveloped virus capsids that does not use cationic lipids, which can affect cytotoxicity.

2. Experimental section

2.1. General

Ultrapure water with high resistivity (>18 MΩ cm), which was purified using the Millipore water purification system (Milli-Q water), was used as a solvent for all experiments. Reversed-phase high-performance liquid chromatography (RP-HPLC) was performed at an ambient temperature using a Shimadzu LC-6AD system equipped with an ultraviolet–visible detector (220 or 551 nm, Shimadzu SPD-10AVvp) and Inertsil WP300 C18 (GL Science) columns (250 × 4.6 or 250 × 20 mm). The proton nuclear magnetic resonance (^{1}H NMR) spectra (600 MHz) were recorded on a Bruker Avance II 600 spectrometer. Matrix-assisted laser desorption/ionization time-of-flight mass spectrometry (MALDI-TOF MS) was performed using UltrafleXtreme or Autoflex T2 instruments (Bruker Daltonics) in the linear/positive mode employing α-cyano-4-hydroxy cinnamic acid (α-CHCA) as the matrix. The electrospray ionization mass spectra (ESI MS) were recorded in a methanol solution using a Q Exactive™ Focus quadrupole/orbitrap hybrid mass spectrometer (Thermo Fisher Scientific) in the positive mode. The reagents were commercially obtained and used without further purification.

2.2. Synthesis

2.2.1. Synthesis of the β-annulus-cysteine peptide

The β-annulus-Cys peptide (H-INHVGGTGGAIMAPVAVTRQLVGSC-OH) was synthesized at a 0.10 mmol scale on H–Cys(Trt)–Trt(2-Cl)–resin (Watanabe Chemical Ind., Ltd.) using manual Fmoc-based coupling reactions. The Fmoc-protected amino

acids (4 eq.) were coupled using (1-cyano-2-ethoxy-2-oxoethylidenaminooxy)dimethylamino–morpholino–carbenium hexafluorophosphate (COMU, 4 eq.) in *N*-methylpyrrolidone (NMP) as the condensing agent and *N,N*-diisopropylethylamine (DIPEA, 8 eq.) in NMP as the base for 2 h at room temperature. Fmoc deprotection was achieved with 20% piperidine in *N,N*-dimethylformamide. The progressions of the coupling reaction and Fmoc deprotection were confirmed by 2,4,6-trinitrobenzene sulfonic acid and a chloranil test kit (Tokyo Chemical Industry Co., Ltd.). The peptidyl resins were washed with NMP and dried in vacuum. The peptide was deprotected and cleaved from the resin by treatment with a cocktail of trifluoroacetic acid (TFA)/water/1,2-ethanedithiol/triisopropylsilane/thioanisole = 3.44/0.2/0.12/0.04/0.2 (mL) at room temperature for 3 h. Afterward, the reaction mixture was filtered to remove the resins, and the filtrate was concentrated in vacuum. The peptide was precipitated by adding methyl *tert*-butyl ether (MTBE) to the residue, after which the supernatant was decanted. After washing three times with MTBE, the crude peptide (154 mg) was lyophilized and purified by RP-HPLC with the elution of a linear gradient of acetonitrile (CH_3CN)/water containing 0.1% TFA (15/85–45/55 over 30 min). The fraction containing the desired peptide was lyophilized to yield a flocculent solid (yield = 30%). MALDI-TOF MS (Figure S1, matrix: α-CHCA): *m/z* = 2409 ($[M + H]^+_{calc.}$ = 2410).

2.2.2. Synthesis of 2-(octyldisulfanyl)-pyridine

Next, 2-(octyldisulfanyl)pyridine (PySS-octyl) was synthesized almost as reported in the literature [36]. Briefly, 2,2'-dithiodipyridine (221 mg, 1.00 mmol) and 1-octanethiol (220 mg, 1.50 mmol) were dissolved in methanol (20 mL). The mixture was stirred at room temperature for 2.5 h, after which the solvent was evaporated under reduced

pressure. The crude product was purified by silica gel column chromatography using chloroform as the eluent to yield 156 mg of PySS-octyl as a viscous liquid (yield = 60.9%). ESI MS (methanol, Figure S2): *m/z* = 256 ($[M + H]^+_{calc.}$ = 256), 278 ($[M + Na]^+_{calc.}$ = 278). ^{1}H NMR (600 MHz, $CDCl_3$) δ 8.45–7.05 (m, 4H), 2.78 (t, 2H, *J* = 7.1 Hz), 1.76 (t, 2H, *J* = 7.1 Hz), 1.29 (t, 2H, *J* = 7.1 Hz), 1.25 (m, 8H), 0.87 (t, 3H, *J* = 7.9 Hz).

2.2.3. Synthesis of the β-annulus–SS-octyl peptide

The β-annulus–SS-octyl peptide (H-INHVGGTGGAIMAPVAVTRQLVGSC–*SS-octyl*) was synthesized by a disulfide-exchange reaction between PySS-octyl and β-annulus–Cys peptide (Figure S3A). A methanol solution (20 mL) of PySS-octyl (18.9 mg, 74.1 μmol) and DIPEA (1.16mg, 8.97 μmol) was added to an aqueous solution (5 mL) of β-annulus–Cys peptide (8.9 mg, 3.69 μmol), after which the mixture was stirred at room temperature for 1 h. After evaporating the solvent under reduced pressure, the crude product was dissolved in dimethylsulfoxide (DMSO). The crude product in DMSO was purified by RP-HPLC with the elution of a linear gradient of CH_3CN/water containing 0.1% TFA (25/75–85/15 over 60 min). The product-containing fraction was lyophilized to yield 4.5 mg of β-annulus–SS-octyl peptide as a flocculent solid (yield = 48%). MALDI-TOF MS (Figure S3, matrix: α-CHCA): *m/z* = 2554 ($[M + H]^+_{calc.}$ = 2554).

2.2.4. Synthesis of the tetramethylrhodamine–β-annulus–SS-octyl peptide

First, an NMP solution (3 mL) of 5-carboxy-tetramethylrhodamine (5-TMR, 4 eq.), COMU (4 eq.), and DIPEA (8 eq.) was added to the protected β-annulus–Cys peptide on the resin that was synthesized as described in Section 2.2.1. The mixture in the plastic column was stirred at room temperature in the darkfor 12 h. Thereafter, the

peptidyl resins were washed with NMP and dichloromethane and dried under vacuum. The peptide was deprotected and cleaved from the resin, following the procedure described in Section 2.2.1. Next, the crude peptide was purified by RP-HPLC with the elution of a linear gradient of CH_3CN/water containing 0.1% TFA (5/95–100/0 over 95 min). The fraction containing the desired peptide was lyophilized to yield the TMR–β-annulus–Cys peptide (*TMR*–INHVGGTGGAIMAPVAVTRQLVGSC–OH) as a flocculent solid (yield = 14%). MALDI-TOF MS (matrix: α-CHCA): *m/z* = 2823 ($[M + H]^+_{calc.}$ = 2823).

The TMR–β-annulus–SS-octyl peptide (*TMR*–INHVGGTGGAIMAPVAVTRQLVGSC–*SS-octyl*) was synthesized by a disulfide-exchange reaction between PySS-octyl and TMR–β-annulus–Cys peptide, following the procedure described in Section 2.2.3. After purification by RP-HPLC with the elution of a linear gradient of CH_3CN/water containing 0.1% TFA (5/95–100/0 over 95 min), 0.61 mg of the β-annulus–SS-octyl peptide was obtained as a red solid (yield = 12%). MALDI-TOF MS (Figure S4, matrix: α-CHCA): *m/z* = 2967 ($[M + H]^+_{calc.}$ = 2968).

2.2.5. Synthesis of the tetramethylrhodamine–β-annulus peptide

The TMR–β-annulus peptide (*TMR*–INHVGGTGGAIMAPVAVTRQLVGSG–OH) was synthesized by condensing 5-TMR into the protected β-annulus peptide on a resin, following the procedure described in Section 2.2.4. The crude product was purified by RP-HPLC with the elution of a linear gradient of CH_3CN/water containing 0.1% TFA (25/75–50/50 over 50 min). The fraction containing the desired peptide was lyophilized to yield TMR–β-annulus peptide as a red flocculent solid (yield = 81%). MALDI-TOF MS (Figure S5, matrix: α-CHCA): *m/z* = 2718 ($[M + H]^+_{calc.}$ = 2719).

2.2.6. Synthesis of tetramethylrhodamine–octyl

Here, 1-octanethiol (2.24 mg, 15 μmol) and tetramethylrhodamine-5-maleimide (0.72 mg, 1.5 μmol) were dissolved in DMSO (1.5 mL), after which the mixture was stirred overnight at room temperature in the dark. Thereafter, the crude product was dissolved in DMSO and purified by RP-HPLC with the elution of a linear gradient of CH_3CN/water containing 0.1% TFA (50/50–85/15 over 70 min) to yield 0.40 mg of TMR–octyl (yield = 43%). ESI MS (methanol, Figure S6): *m/z* = 628 ($[M + H]^+_{calc.}$ = 628); ^{1}H NMR (600 MHz, CD_3OD) δ 8.29 (d, 1H, *J* = 1.5 Hz), 7.81 (d, 1H, *J* = 7.5 Hz), 7.53 (dd, 1H, *J* = 7.5, 1.5 Hz), 7.20 (d, 1H, *J* = 7.5 Hz), 7.19 (d, 1H, *J* = 7.5 Hz), 7.07 (d, 1H, *J* = 10.1 Hz), 7.05 (d, 1H, *J* = 1.5 Hz), 6.97 (d+s, 2H, *J* = 10.1 Hz),4.09 (dd 1H, *J* = 8.4, 2.5 Hz), 2.97 (dd 1H, *J* = 12.4, 2.5 Hz), 2.83 (dd 1H, *J* = 12.4, 8.4 Hz), 1.72 (m, 2H), 1.48–1.26 (m, 12H), 0.87 (t, 3H, *J* = 7.9 Hz).

2.3. Preparation of the alkyl anchor–modified artificial viral capsid

A stock solution (2 mM) of the β-annulus–SS-octyl peptide in DMSO was diluted 20 times with a 10 mM Tris-HCl buffer (pH 7.4) to prepare a 100 μM peptide solution in the 10 mM Tris-HCl buffer containing 5% DMSO (pH 7.4). The 100 μM peptide solution was further diluted with the 10 mM Tris-HCl buffer containing 5% DMSO (pH 7.4) to prepare 75–0.5 μM peptide solutions. Each solution was vortexed for 10 s, ultrasonicated for 10 s, and incubated for 20 min at 25°C.

2.4. Preparation of the enveloped artificial viral capsid

A stock solution of 1-palmitoyl-2-oleoyl-*sn*-glycero-3-phosphocholine (POPC) in chloroform (10 mM, 75 μL), methanol (75 μL), and chloroform (150 μL) was placed in a glass tube and dried under vacuum for 6 h. The resulting lipid film was hydrated with

the 50 μM β-annulus–SS-octyl peptide in the 10 mM Tris-HCl buffer containing 5% DMSO (pH 7.4) by shaking at 25°C for 5 min. The excess lipid was removed by ultracentrifugation (67,000 rpm, 5 min, Optima MAX-TL ultracentrifuge, Beckman Coulter) at 25°C to obtain a solution of enveloped artificial viral capsid (final concentration: [β-annulus–SS-octyl] = 50 μM, [POPC] = 5 mM).

2.5. Dynamic light scattering and ζ-potential

The dynamic light scattering (DLS) measurements of the alkyl anchor–modified artificial viral capsids, enveloped artificial viral capsids, and POPC vesicles in the 10 mM Tris-HCl buffer containing 5% DMSO (pH 7.4) were obtained at 25°C using a Zetasizer Nano ZS (Malvern) with an incident He–Ne laser (633 nm) and a ZEN2112 low-volume glass cuvette cell. Count rates (sample scattering intensities) were provided during the measurements. The correlation time for the scattered light intensity, $G(\tau)$, was measured several times, and the averaged results were fitted into Equation (1), where B, A, q, t, and D are the baseline, amplitude, scattering vector, delay time, and diffusion coefficient, respectively:

$$G(\tau) = B + A \cdot \exp(-2q^2 D\tau) \quad (1)$$

The hydrodynamic radius (R_H) of the scattering peptides was calculated by the Stokes–Einstein equation (Equation (2)), where η, k_B, and T are the solvent viscosity, Boltzmann's constant, and absolute temperature, respectively:

$$R_H = \frac{k_B T}{6\pi\eta D} \quad (2)$$

Further, the ζ-potentials of each sample were measured at 25°C using the Zetasizer Nano ZS (Malvern) with a DTS1070 clear disposable zeta cell.

2.6. Transmission electron microscopy

Aliquots (5 μL) of the samples were applied to hydrophilized carbon-coated Cu-grids (C-SMART Hydrophilic transmission emission microscopy (TEM) grids, Alliance Biosystems) for 1 min and removed. Subsequently, the TEM samples were stained with an EM stainer aqueous solution (Nisshin EM Co., Ltd., 5 μL), for 10 min and removed. After drying the sample-loaded grids under vacuum, they were observed by TEM (JEOL JEM 1400 Plus) at an accelerating voltage of 80 kV.

2.7. Fluorescence spectroscopy

The enveloped artificial viral capsid comprising 1,2-dioleoyl-*sn*-glycero-3-phosphoethanolamine-*N*-(7-nitro-2-1,3-benzoxadiazol-4-yl) (NBD-PE, 10 μM) as the donor, POPC (4.99 mM), *β*-annulus–SS-octyl (25, 23.1 μM) peptide, and TMR–β-annulus–SS-octyl peptide (0, 1.9 μM) as the acceptor in the 10 mM Tris-HCl buffer containing 5% DMSO was constructed, following the procedure described in Section 2.4. The total concentrations of the unlabeled *β*-annulus–SS-octyl peptide and TMR–β-annulus–SS-octyl peptide were kept constant (25 μM). The fluorescence emission spectra (500–650 nm) obtained from exciting the samples at 460 nm were measured at 25°C using a Jasco FP 8200 fluorescence spectrometer (JASCO Co., Ltd.). The fluorescence resonance energy transfer (FRET) efficiency at a certain donor and acceptor ratio, E, was calculated by Equation (3), where I_D and I_{DA} are the fluorescence intensities of the donor without and with the acceptor, respectively [37]:

$$E = 1 - \frac{I_{DA}}{I_D} \quad (3)$$

The distance, R, between the donor and acceptor was calculated by Equation (4), where R_0 is the Förster radius of the NBD/TMR pair. It was set to R_0 = 5.1 nm, following the

literature [38].

$$R = R_0 \left(\frac{1-E}{E}\right)^{\frac{1}{6}} \quad (4)$$

2.8. Preparation of giant unilamellar vesicles

GUVs comprising POPC, NBD-PE, and cholesterol were prepared by the water-in-oil (w/o) emulsion centrifugation method [39-42]. Stock chloroform solutions of POPC (10 mM, 25 μL) and cholesterol (10 mM, 5 μL) were mixed in a microtube with organic solvent resistance, after which the solvent was evaporated by flowing nitrogen gas. A chloroform solution of NBD-PE (0.1 mM, 50 μL) and liquid paraffin (500 μL) were added to the mixture, after which it was incubated at 80°C for 30 min in a dry aluminum heating bath to evaporate chloroform. As the inner aqueous phase of GUV, an aqueous solution (45 μL) of 150 mM sucrose and 350 mM glucose in a 10 mM 4-(2-hydroxyethyl)-1-piperazineethanesulfonic acid (HEPES) buffer (pH 7.4) was added to the mixture in liquid paraffin. Thereafter, the mixture was vortexed for 30 s and incubated in ice for 10 min to obtain the w/o emulsion. Further, the w/o emulsion (400 μL) was gently layered on the upper surface of 500 mM glucose in the 10 mM HEPES buffer (pH 7.4, 400 μL) at 4°C in a lidded microtube. The w/o emulsion was precipitated by ultracentrifugation (15,600 × *g*) at 4°C for 30 min, and the supernatant liquid paraffin was subsequently removed. The obtained pellet (20 μL) was collected in another microtube, after which an aqueous solution of 500 mM glucose in the 10 mM HEPES buffer containing 5% DMSO (pH 7.4) was added as the outer aqueous solution of GUV. After the GUV dispersion was incubated at 25°C for 2 h, the fluorescence images of GUV on poly-lysine/bovine serum albumin (BSA)-coated glass slides were observed by confocal laser scanning microscopy (CLSM) using FluoView FV10i (Olympus). NBD-PE was excited at 473 nm and observed through a 490–540 nm

emission band-pass filter.

2.9. Interaction of the alkyl anchor–modified artificial viral capsids with GUVs

2.9.1. Addition of the alkyl anchor–modified capsids outside GUV

When a GUV solution containing the alkyl anchor–modified capsids outside was prepared by the w/o emulsion centrifugation method (Section 2.8), an aqueous solution of 2 μM TMR–β-annulus–SS-octyl and 500 mM glucose in a 10 mM HEPES buffer containing 5% DMSO (pH 7.4) was used as the outer aqueous phase of GUV. The interaction between GUV and the alkyl anchor–modified artificial viral capsids added outside GUV was observed by CLSM on poly-lysine/BSA-coated glass slides. TMR was excited at 551 nm and observed through a 574 nm emission band-pass filter. As control experiments, GUVs with 2 μM TMR–β-annulus or 2 μM TMR–SS-octyl added outside were also prepared and observed by CLSM.

2.9.2. Addition of the alkyl anchor–modified capsids inside GUV

When GUV encapsulating the alkyl anchor–modified capsids was prepared by the w/o emulsion centrifugation method (Section 2.8), an aqueous solution of 2 μM TMR–β-annulus–SS-octyl, 150 mM sucrose, and 350 mM glucose in the 10 mM HEPES buffer containing 5% DMSO (pH 7.4) was used as the inner aqueous phase of GUV. The interaction between GUV and the encapsulated alkyl anchor–modified artificial viral capsids was observed on poly-lysine/BSA-coated glass slides by CLSM. As control experiments, GUVs encapsulating 2 μM TMR–β-annulus or 2 μM TMR–SS-octyl were also prepared and observed by CLSM.

2.9.3. TEM observation of GUV following the addition of the alkyl anchor–modified capsids

Herein, aliquots (5 μL) of aqueous solutions of GUV containing the alkyl anchor–modified capsids outside or GUV encapsulating the alkyl anchor–modified capsids in the 10 mM HEPES buffer containing 5% DMSO (pH 7.4) were applied to hydrophilized carbon-coated Cu-grids (Alliance Biosystems) for 1 min and subsequently removed. Thereafter, the TEM samples were stained using an EM stainer aqueous solution (Nisshin EM Co., Ltd., 5 μL), for 10 min and removed. The sample-loaded grids dried under vacuum were then observed by TEM (JEOL JEM 1400 Plus) at an accelerating voltage of 80 kV.

3. Results and discussion

3.1. Synthesis and self-assembly of the β-annulus–SS-octyl peptide

A β-annulus–Cys peptide (INHVGGTGGAIMAPVAVTRQLVGSC) containing Cys at the C-terminus was synthesized by standard Fmoc-based solid-phase methods. The β-annulus–SS-octyl peptide was synthesized by the disulfide-exchange reaction of the β-annulus–Cys peptide with PySS-octyl, purified by RP-HPLC, and confirmed by MALDI-TOF MS (*m/z* = 2554 $[M + H]^+$, Figure S3). Owing to the β-annulus–SS-octyl peptide being poorly soluble in water, a stock solution of the peptide in DMSO was prepared. The stock solution of the DMSO-dissolved β-annulus–SS-octyl peptide self-assembled, following its dilution with the 10 mM Tris-HCl buffer (pH 7.4, Figure 2A). The DLS measurements of the β-annulus–SS-octyl peptide (50 μM) in the buffer containing 5% DMSO displayed the formation of assemblies with sizes of 34.0 ± 0.5 and 211 ± 27 nm (Figure 2B). The TEM images displayed the formation of ~200 nm aggregates comprising spherical structures with a size range of 30–80 nm (Figure 2C).

The complete removal of DMSO facilitated further aggregation of the peptide. The ζ-potential of the β-annulus–SS-octyl peptide assemblies at pH 7.4 was −11.5 ± 2.6 mV (Figure 2D). As unmodified β-annulus peptides form spherical assemblies with sizes of 30–50 nm [18], these results indicated the formation of ~200 nm aggregates via the hydrophobic interactions among the octyl chains displayed on the outer surface of the artificial viral capsid. Despite insufficient evidence indicating hollowness of the components of the aggregates, we believe the aggregates comprised hollow artificial viral capsids.

3.2. Complexation of the alkyl anchor–modified artificial viral capsids with lipids

The complexation of the alkyl anchor–modified artificial viral capsid aggregates with the zwitterionic lipid, POPC, formed highly dispersed spherical assemblies with sizes of 64.1 ± 21.0 nm (Figure 2E). The TEM image of the complex revealed deeply stained spherical structures (diameter = ~58 nm) covered with thinly stained fringe structures with a thickness of ~6.8 nm (Figure 2F). The ζ-potential of the complex (−1.6 ± 0.2 mV, Figure 2G) shifted positively compared with that of the alkyl anchor–modified artificial viral capsid (Figure 2D). These results indicated that the enveloped artificial viral capsid was formed by the hydrophobic interactions between the alkyl anchor–modified artificial viral capsid and POPC lipid membrane. Contrarily, POPC without the β-annulus–SS-octyl peptide formed larger spherical vesicles compared with the enveloped artificial viral capsids (Figures 2H, I), reflecting the compaction of the vesicle membrane by the alkyl anchor–modified artificial viral capsid present therein. The results in which the ζ potentials of the enveloped artificial viral capsid and POPC vesicle were almost neutral (Figures 2G, J) confirmed that the surface of the enveloped

artificial viral capsid was covered with POPC.

The dependence of the peptide concentration on the DLS-obtained scattering intensity revealed that the critical aggregation concentration (CAC) of the alkyl anchor–modified artificial viral capsid was 5 μM (Figure 3A), whereas that of the enveloped artificial viral capsid via hydrophobic interactions was 0.25 μM (Figure 3B). The CAC value was comparable with that of the previously reported enveloped artificial viral capsid obtained via electrostatic interactions (the CAC was 0.25 μM) [28]. This indicated that the self-assembled artificial viral capsid from the β-annulus–SS-octyl peptide was stabilized by complexing with the lipid bilayer via hydrophobic interactions, similar to the case involving electrostatic interactions.

A fluorescence-labeled enveloped viral capsid was constructed by complexing a TMR-labeled artificial viral capsid with a nitrobenzoxadiazole (NBD)-labeled lipid bilayer (Figure 4A). The TMR-labeled artificial viral capsid co-assembled from the TMR-labeled β-annulus–SS-octyl peptide (Figure S4) and β-annulus–SS-octyl peptide (0/25 and 1.9/23.1 molar ratios, respectively) were complexed with a lipid film of POPC/NBD-PE (499/1 molar ratio) to yield their complexes exhibiting sizes of ~90 nm. The fluorescence spectral change observed as NBD on the envelope was excited in the presence of different concentrations of the TMR-labeled β-annulus–SS-octyl peptide indicated that FRET proceeded from the donor NBD to the acceptor TMR (Figure 4B). The FRET efficiency, *E*, as estimated from the fluorescence intensity ratio of the donor, was 0.59, and the calculated average distance between the donor and acceptor was 4.8 nm. These results confirmed the proximity of lipids and the β-annulus–SS-octyl peptide in the enveloped viral capsid. Considering the changes in the particle size distribution, ζ potential (Figure 2), and FRET results (Figure 4), we conclude that the enveloped artificial virus capsid was covered with a lipid bilayer membrane. Therefore, we

demonstrated that stable enveloped viral capsids can also be constructed via the hydrophobic interactions between the alkyl anchors on the capsid surface and lipid bilayer, similar to the previously reported formation via the electrostatic interactions between the anionic capsid and cationic lipid bilayer [28].

3.3. Budding outside-to-inside giant vesicles

As described above, the alkyl anchor–modified artificial viral capsids interacted with the lipid membrane to form enveloped viral capsids. Next, we evaluated the interaction of the alkyl anchor–modified artificial viral capsids with GUVs by fluorescence imaging. NBD-labeled GUVs comprising POPC/cholesterol/NBD-PE (100/10/1 molar ratio) were prepared by the w/o emulsion centrifugation method. The presence of cholesterol facilitated the stable preparation of relatively large GUVs. The NBD-derived fluorescence image revealed the formation of spherical GUVs with sizes of 5–10 μm (Figure 5A). Interestingly, following the addition of 2 μM TMR–β-annulus-SS-octyl to the outer aqueous phase of GUV, daughter vesicles (size = 2–3 μm) encapsulating TMR fluorescence were observed inside GUVs (Figure 5B), indicating that the daughter vesicles containing aggregates of the alkyl anchor–modified artificial viral capsids bud outside-to-inside GUVs. As CAC of β-annulus–SS-octyl was 5 μM (Figure 3A), TMR–β-annulus–SS-octyl at 2 μM should exist as dissociated peptides in the outer phase. The time-series CLSM images indicated the immediate occurrence of concave deformation toward the inside of the GUV, followed by detachment of daughter vesicles inside the GUV (Figure 5C). Presumably, the anchoring of the octyl chains to the lipid bilayer outside GUV induces self-assembling to form artificial viral capsids on the membrane. The aggregation of the alkyl anchor–modified artificial viral capsids on the GUV membrane might have induced curvature changes in the GUV membrane, facilitating the budding of the daughter vesicle encapsulating the capsids outside-to-inside GUV.

The TEM images of the NBD-labeled vesicles without TMR–β-annulus–SS-octyl revealed the presence of small spherical structures (sizes <1 μm) attributed to the shrinkage of the vesicles during sample drying (Figure S7). Following the addition of TMR–β-annulus–SS-octyl to the outer aqueous phase of GUV, the TEM images displayed dark-stained spherical structures inside the shrunk vesicles (Figures 6A–C). This result also supports fact that capsids formed outside the GUV were stained and budded daughter vesicles that encapsulated capsids outside-to-inside the mother vesicle.

We calculated the ratio of the number of deformed GUVs of the more than 100 GUVs, following the addition of 2 μM TMR-β-annulus-SS-octyl, TMR–β-annulus, or TMR–octyl outside the GUVs (Figures 7, and S8–10). When TMR-β-annulus-SS-octyl was added to the outer aqueous phase of GUV, 24.1% of GUVs were observed to bud, of which a few GUVs budded at two locations (Figure S8). Conversely, the addition of the TMR–β-annulus peptide without an alkyl anchor to the outer aqueous phase of GUV facilitated minimal budding or GUV deformation (Figures S9 and S11). The addition of TMR–octyl without the β-annulus peptide to the outer aqueous phase of GUV resulted in certain degree (6.3%) of budding of GUVs. However, in several cases, CLSM images revealed the co-localization of the TMR and NBD fluorescence (Figures S10 and S12). The lower NBD intensity on the GUVs suggested the increased occurrence of FRET from NBD to TMR on the membrane. This may be attributed to a greater number of TMR–octyl molecules being anchored to the membrane. Although TMR–octyl was anchored to GUV, it was less effective in inducing budding or GUV deformation compared to TMR-β-annulus-SS-octyl. These results indicate that the β-annulus peptide and octyl chain are required to facilitate the effective budding of daughter vesicles encapsulating capsids outside-to-inside GUV.

The budding of the daughter vesicle outside-to-inside GUV, following the

addition of TMR–β-annulus–SS-octyl was significantly affected by the membrane fluidity (Figures 8 and S13). GUVs comprising 1,2-dioleoyl-sn-glycero-3-phosphocholine (DOPC; gel–liquid crystal phase transition temperature (T_c) = –20°C) or POPC (T_c = –2°C) [43] with high fluidity induced the budding of the daughter vesicle outside-to-inside GUVs, following the addition of TMR–β-annulus–SS-octyl. Conversely, the addition of TMR–β-annulus–SS-octyl outside GUV comprising dipalmitoylphosphatidylcholine (DPPC; T_c = 41°C) with low fluidity revealed only the accumulation of capsids on the membrane, barely inducing budding and GUV deformation. These differences may be attributed to the anchoring efficiency of the octyl groups and the ease of membrane deformation based on the differences in membrane fluidity. Furthermore, the addition of the TMR–β-annulus peptide barely induced budding or deformation of any GUVs regardless of the membrane fluidity. The addition of TMR–octyl was often observed to anchor to the membrane. Consequently, fewer GUVs were budded compared to TMR-β-annulus-SS-octyl.

3.4. Budding inside-to-outside giant vesicle

GUVs encapsulating the alkyl anchor–modified artificial viral capsids were prepared by adding 2 μM TMR–β-annulus–SS-octyl in the inner aqueous phase of GUV using the w/o emulsion centrifugation method. Contrary to when TMR–β-annulus–SS-octyl was added to the outer aqueous phase of GUV, the budding of the daughter vesicles (size = 1–2 μm) encapsulating TMR-derived fluorescence was observed outside GUVs (Figure 9), indicating that the daughter vesicles containing aggregates of the alkyl anchor–modified artificial viral capsids bud inside-to-outside GUVs. The daughter vesicle shown in Figure 9B did not completely detach from their mother GUVs, remaining attached to them. An intermediate state may have emerged during GUV detachment or

sufficient membrane deformation was not induced by the alkyl anchor–modified artificial viral capsids for the detachment. The time-series CLSM images exhibited the convex deformation of GUV followed by detachment of daughter vesicles from the parent vesicles (Figure 9C). The budding of the daughter vesicle inside-to-outside GUV might be induced by the anchoring of the octyl chains to the lipid bilayer inside GUV, followed by self-assembling, to form artificial viral capsids on the membrane. The TEM images of the vesicles encapsulating the alkyl anchor–modified artificial viral capsids also supported the budding of the daughter vesicle inside-to-outside the mother vesicles (Figures 6D–6F). Thus, the capsids formed inside the mother vesicles were not observed as dark-stained images owing to the staining agent not penetrating through the membrane.

The ratio of the number of deformed GUVs encapsulating TMR-β-annulus-SS-octyl more often (21.7%) than TMR–octyl (11.3%). Whereas, TMR-β-annulus barely induced deformation (Figure 10). The budding inside-to-outside GUV was also significantly affected by the membrane fluidity of GUV (Figures 11, and S17–S19). The budding inside-to-outside GUVs comprising DOPC or POPC with high fluidity was induced by the encapsulation of TMR–β-annulus–SS-octyl, whereas GUV comprising DPPC with low fluidity barely induced budding and GUV deformation. Furthermore, GUV comprising DOPC induced budding, albeit at a low frequency, even when encapsulating TMR–β-annulus without an alkyl anchor. Contrarily, TMR–β-annulus-encapsulating GUVs comprising POPC or DPPC minimally induced budding. Although TMR–octyl often induced anchoring to the lipid bilayer, fewer GUVs were budded compared to TMR-β-annulus-SS-octyl. Consequently, the anchoring efficiency was increased with the increasing membrane fluidity. These results indicate that the β-annulus peptide and octyl chain are required for the budding of daughter vesicles

encapsulating capsids inside-to-outside GUVs. Further the efficiency increased with the increasing fluidity of the GUV membrane. Thus, as reduced cholesterol concentration increases GUV membrane fluidity, the efficiency of budding of the capsids-encapsulating daughter vesicle may be controlled by changing cholesterol concentration.

4. Conclusions

We designed a simple molecule, a β-annulus peptide alkylated at the C-terminus, to construct an artificial viral capsid system budding from the lipid bilayer of GUV. The β-annulus peptide bearing an octyl chain at the C-terminus, which was synthesized by the disulfide-exchange reaction, self-assembled into an artificial virus capsid bearing an alkyl anchor on the surface. Although the alkyl anchor–modified capsids aggregated via hydrophobic interactions, dispersed enveloped artificial viral capsids were formed by the anchoring of the octyl chain to the lipid bilayer. The addition of the β-annulus peptide bearing an octyl chain to the outer aqueous phase of GUV induced the budding of the daughter vesicle encapsulating capsids outside-to-inside the mother GUV. Conversely, the encapsulation of the β-annulus peptide bearing an octyl chain in the inner aqueous phase of GUV induced the budding of the daughter vesicle encapsulating capsids inside-to-outside the mother GUV. The budding of the daughter vesicle encapsulating capsids outside-to-inside and inside-to-outside GUV was significantly affected by the membrane fluidity.

In this study, we presented a novel guideline for designing artificial viral capsid budding inside and outside the GUV membrane. The simple virus-mimicking material developed in this study, which buds off through membrane anchoring, offers physicochemical insights into the mechanisms of natural virus budding from cells. Previous studies reported that the deformation and perforation of GUV by nanoparticles

was attributable to an increase in the surface tension on the membrane via a steric crowding mechanism following nanoparticle adhesion to the membrane [44]. The proposed artificial virus capsid budding system can be explained via a similar presumed mechanism: the budding of capsids from GUV were induced by an increase in the surface tension on the membrane owing to the aggregation of capsids following the adhesion of capsids to the membrane. Further detailed studies on the effect of various factors such as GUV size, peptide concentration, alkyl anchor length, and alkyl anchor density of the capsid on GUV budding can aid in understanding the physicochemical mechanism of budding. Artificial virus capsids based on the self-assembly of β-annulus peptides are advantageous as they can undergo various molecular modifications. We envision the construction of an artificial virus system that localizes on membranes and buds out from the cells in response to external stimuli. Such a stimulus-responsive artificial virus budding system can be applied to intercellular molecular transport and communication systems, drug delivery, in-cell component recovery, and the control of cell function.

Disclosure statement

No potential conflict of interest was reported by the author(s).

Funding

This work was supported by a Grant-in-Aid for Scientific Research (B) (JSPS KAKENHI Grant No. JP22H02199) and a Grant-in-Aid for Transformative Research Areas (A) “Molecular Cybernetics” (JSPS KAKENHI Grant No. JP20H05970).

References

[1] Rheinemann L, Sundquist WI. Virus. Budding. In: Bamford, DH, Zuckerman, M,

editors. Encyclopedia of Virology. Cambridge, MA, USA: Academic Press; 2021. p. 519–528. doi: 10.1016/B978-0-12-814515-9.00023-0.

[2] Garoff H, Hewson R, Opstelten DJ. Virus maturation by budding. Microbiol Mol Biol Rev. 1998;62(4):1171–1190. doi: 10.1128/MMBR.62.4.1171-1190.1998.

[3] Sundquist WI, Kräusslich HG. HIV-1 assembly, budding, and maturation. Cold Spring Harb Perspect Med. 2012;2(7):a006924. doi: 10.1101/cshperspect.a006924.

[4] Grigorov B, Muriaux D, Argirova R, et al. New insights into human immunodeficiency virus—type 1 replication. Biotechnol Biotechnol Equip. 2005;19(1):3–15. doi: 10.1080/13102818.2005.10817147.

[5] Rossman JS, Lamb RA. Influenza virus assembly and budding. Virology. 2011;411(2):229–236. doi: 10.1016/j.virol.2010.12.003.

[6] Lipowsky R. Multispherical shapes of vesicles highlight the curvature elasticity of biomembranes. Adv Colloid Interface Sci. 2022;301:102613. doi: 10.1016/j.cis.2022.102613.

[7] Long MS, Cans AS, Keating CD. Budding and asymmetric protein microcompartmentation in giant vesicles containing two aqueous phases. J Am Chem Soc. 2008;130(2):756–762. doi: 10.1021/ja077439c.

[8] Andes-Koback M, Keating CD. Complete budding and asymmetric division of primitive model cells to produce daughter vesicles with different interior and membrane compositions. J Am Chem Soc. 2011;133(24):9545–9555. doi: 10.1021/ja202406v.

[9] Li Y, Kusumaatmaja H, Lipowsky R, et al. Wetting-induced budding of vesicles in contact with several aqueous phases. J Phys Chem B. 2012;116(6):1819–1823. doi: 10.1021/jp211850t.

[10] Yu Y, Vroman JA, Bae SC, et al. Vesicle budding induced by a pore-forming peptide. J Am Chem Soc. 2010;132(1):195–201. doi: 10.1021/ja9059014.

[11] Castro JM, Sugiyama H, Toyota T. Budding and division of giant vesicles linked to phospholipid production. Sci Rep. 2019;9(1):165. doi: 10.1038/s41598-018-36183-9.

[12] Wen HY, Zhu H, Wen HP, et al. Artificial cells for cellular behavior mimicry induced by sphingomyelin degradation. Bioconjug Chem. 2023;34(6):1037–1044. doi: 10.1021/acs.bioconjchem.3c00123.

[13] de Souza Melchiors MS, Ivanov T, Harley I, et al. Membrane manipulation of giant unilamellar polymer vesicles with a temperature-responsive polymer. Angw Chem Int. Ed. 2022;61(39):e202207998. doi: 10.1002/anie.202207998.

[14] Steinkühler J, Knorr RL, Zhao Z, et al. Controlled division of cell-sized vesicles by low densities of membrane-bound proteins. Nat Commun. 2020;11(1):905. doi: 10.1038/s41467-020-14696-0.

[15] De Franceschi N, Pezeshkian W, Fragasso A, et al. Synthetic membrane shaper for controlled liposome deformation. ACS Nano. 2023;17(2):966–978. doi: 10.1021/acsnano.2c06125.

[16] Gui D, Gupta S, Xu J, et al. A novel minimal in vitro system for analyzing HIV-1 Gag-mediated budding. J Biol Phys. 2015;41(2):135–149. doi: 10.1007/s10867-014-9370-z.

[17] Matsuura K. Synthetic approaches to construct viral capsid-like spherical nanomaterials. Chem Commun. 2018;54(65):8944–8959. doi: 10.1039/C8CC03844A.

[18] Matsuura K, Watanabe K, Matsuzaki T, et al. Self-assembled synthetic viral capsids from a 24-mer viral peptide fragment. Angw Chem Int. Ed. 2010;49(50):9662–9665. doi: 10.1002/anie.201004606.

[19] Matsuura K, Watanabe K, Matsushita Y, et al. Guest-binding behavior of peptide nanocapsules self-assembled from viral peptide fragments. Polym J. 2013;45(5):529–534. doi: 10.1038/pj.2012.235.

[20] Nakamura Y, Sato Y, Inaba H, et al. Encapsulation of mRNA into artificial viral capsids via hybridization of a β-annulus-dT_{20} conjugate and the poly(A) tail of mRNA. Appl Sci. 2020;10(22):8004. doi: 10.3390/app10228004.

[21] Matsuura K, Nakamura T, Watanabe K, et al. Self-assembly of Ni-NTA-modified β-annulus peptides into artificial viral capsids and encapsulation of His-tagged proteins. Org Biomol Chem. 2016;14(33):7869–7874. doi: 10.1039/C6OB01227B.

[22] Sakamoto K, Furukawa H, Arafiles JVV, et al. Artificial nanocage formed via self-assembly of β-annulus peptide for delivering biofunctional proteins into cell interiors. Bioconjug Chem. 2022;33(2):311–320. doi: 10.1021/acs.bioconjchem.1c00534.

[23] Matsuura K. Dressing up artificial viral capsids self-assembled from C-terminal-modified β-annulus peptides. Polym J. 2020;52(9):1035–1041. doi: 10.1038/s41428-020-0355-4.

[24] Matsuura K, Honjo T. Artificial viral capsid dressed up with human serum albumin. Bioconjug Chem. 2019;30(6):1636–1641. doi: 10.1021/acs.bioconjchem.9b00327.

[25] Matsuura K, Ota J, Fujita S, et al. Construction of ribonuclease-decorated artificial virus-like capsid by peptide self-assembly. J Org Chem. 2020;85(3):1668–1673. doi: 10.1021/acs.joc.9b02295.

[26] Liang Y, Furukawa H, Sakamoto K, et al. Anticancer activity of reconstituted ribonuclease S-decorated artificial viral capsid. ChemBioChem. 2022;23(15):e202200220. doi: 10.1002/cbic.202200220.

[27] Sakamoto K, Uchiyama K, Iwasaki T, et al. An artificial viral capsid decorated with a DNA aptamer internalizing into lymphoma cells. J Mater Chem B. 2023;11(26):6053–6059. doi: 10.1039/D3TB00169E.

[28] Furukawa H, Inaba H, Inoue F, et al. Enveloped artificial viral capsids self-assembled from anionic β-annulus peptide and cationic lipid bilayer. Chem Commun. 2020;56(52):7092–7095. doi: 10.1039/D0CC02622K.

[29] Furukawa H, Inaba H, Sasaki Y, et al. Embedding a membrane protein into an enveloped artificial viral replica. RSC Chem Biol. 2022;3(2):231–241. doi:

10.1039/D1CB00166C.

[30] Ito K, Furukawa H, Inaba H, et al. Antigen/adjuvant-displaying enveloped viral replica as a self-adjuvanting anti-breast-cancer vaccine candidate. J Am Chem Soc. 2023;145(29):15838–15847. doi: 10.1021/jacs.3c02679.

[31] Furukawa H, Kimura Y, Inaba H, et al. A supramolecular system mimicking the infection process of an enveloped virus through membrane fusion. Sci Rep. 2023;13(1):19934. doi: 10.1038/s41598-023-47347-7.

[32] Otake S, Okuro K, Bochicchio D, et al. Nitrobenzoxadiazole-appended cell membrane modifiers for efficient optoporation with noncoherent light. Bioconjug Chem. 2018;29(6):2068–2073. doi: 10.1021/acs.bioconjchem.8b00270.

[33] Feng L, Xie Y, Au-Yeung SK, et al. A fluorescent molecular rotor probe for tracking plasma membranes and exosomes in living cells. Chem Commun. 2020;56(60):8480–8483. doi: 10.1039/D0CC03069D.

[34] Nakamura A, Katahira R, Sawada S, et al. Chemogenetic control of protein anchoring to endomembranes in living cells with lipid-tethered small molecules. Biochemistry. 2020;59(2):205–211. doi: 10.1021/acs.biochem.9b00807.

[35] Uchida K, Obayashi H, Minamihata K, et al. Artificial palmitoylation of proteins controls the lipid domain-selective anchoring on biomembranes and the raft-dependent cellular internalization. Langmuir. 2022;38(31):9640–9648. doi: 10.1021/acs.langmuir.2c01205.

[36] Du Y, He W, Zhou W, et al. Disulfide phosphatidylcholines: alternative phospholipids for the preparation of functional liposomes. Chem Commun. 2019;55(58):8434–8437. doi: 10.1039/C9CC03571K.

[37] Lakowicz JR. Principles of Fluorescence Spectroscopy, 3rd Ed., New York: Springer, 2006. p. 443–475.

[38] Schneggenburger PE, Müllar S, Worbs B, et al. Molecular recognition at the membrane−water interface: controlling integral peptide helices by off-membrane nucleobase pairing. J Am Chem Soc 2010;132(23):8020–8028. doi: 10.1021/ja1006349.

[39] Natsume Y, Toyota T. Giant vesicles containing microspheres with high volume fraction prepared by water-in-oil emulsion centrifugation. Chem Lett. 2013;42(3):295–297. doi: 10.1246/cl.2013.295.

[40] Natsume Y, Wen HI, Zhu T, et al. Preparation of giant vesicles encapsulating microspheres by centrifugation of a water-in-oil emulsion. J Vis Exp. 2017;119(119):e55282. doi: 10.3791/55282.

[41] Pautot S, Frisken BJ, Weitz DA. Engineering asymmetric vesicles. Proc Natl Acad Sci U S A. 2003;100(19):10718–10721. doi: 10.1073/pnas.1931005100.

[42] Pautot S, Frisken BJ, Weitz DA. Production of unilamellar vesicles using an inverted emulsion. Langmuir. 2003;19(7):2870–2879. doi: 10.1021/la026100v.

[43] Liu H, Bachand GD, Kim H, et al. Lipid nanotube formation from streptavidin−membrane binding. Langmuir. 2008;24(8):3686–3689. doi: 10.1021/la704018s.

[44] Li S, Malmstadt N. Deformation and poration of lipid bilayer membranes by cationic nanoparticles. Soft Matter. 2013;9(20):4969–4976. doi: 10.1039/C3SM27578G.

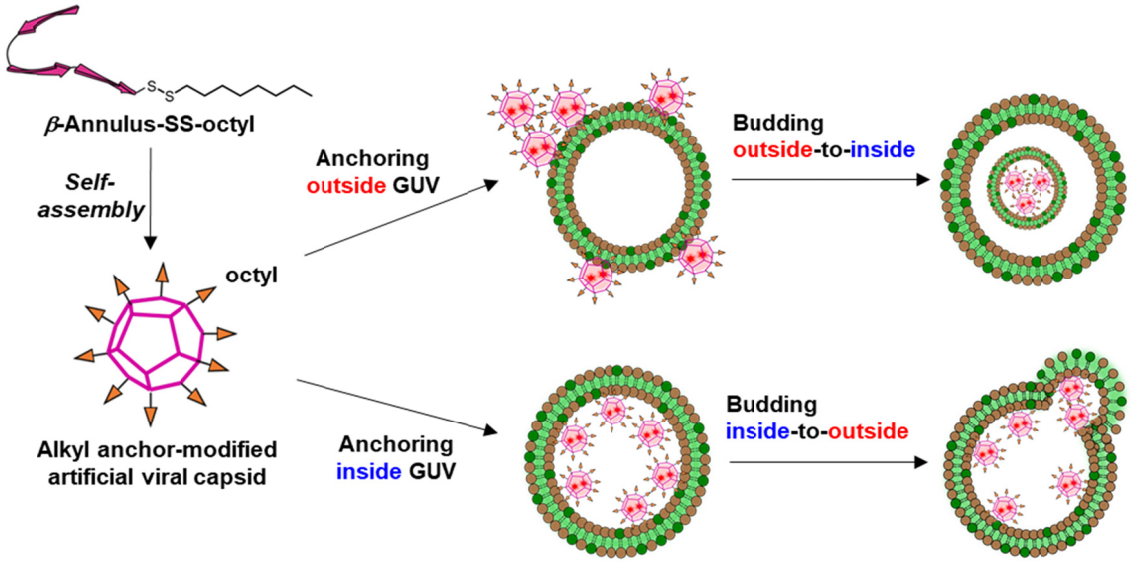

Figure 1. Schematic illustration of the alkyl anchor-modified artificial viral capsid budding outside-to-inside and inside-to-outside giant unilamellar vesicles (GUVs).

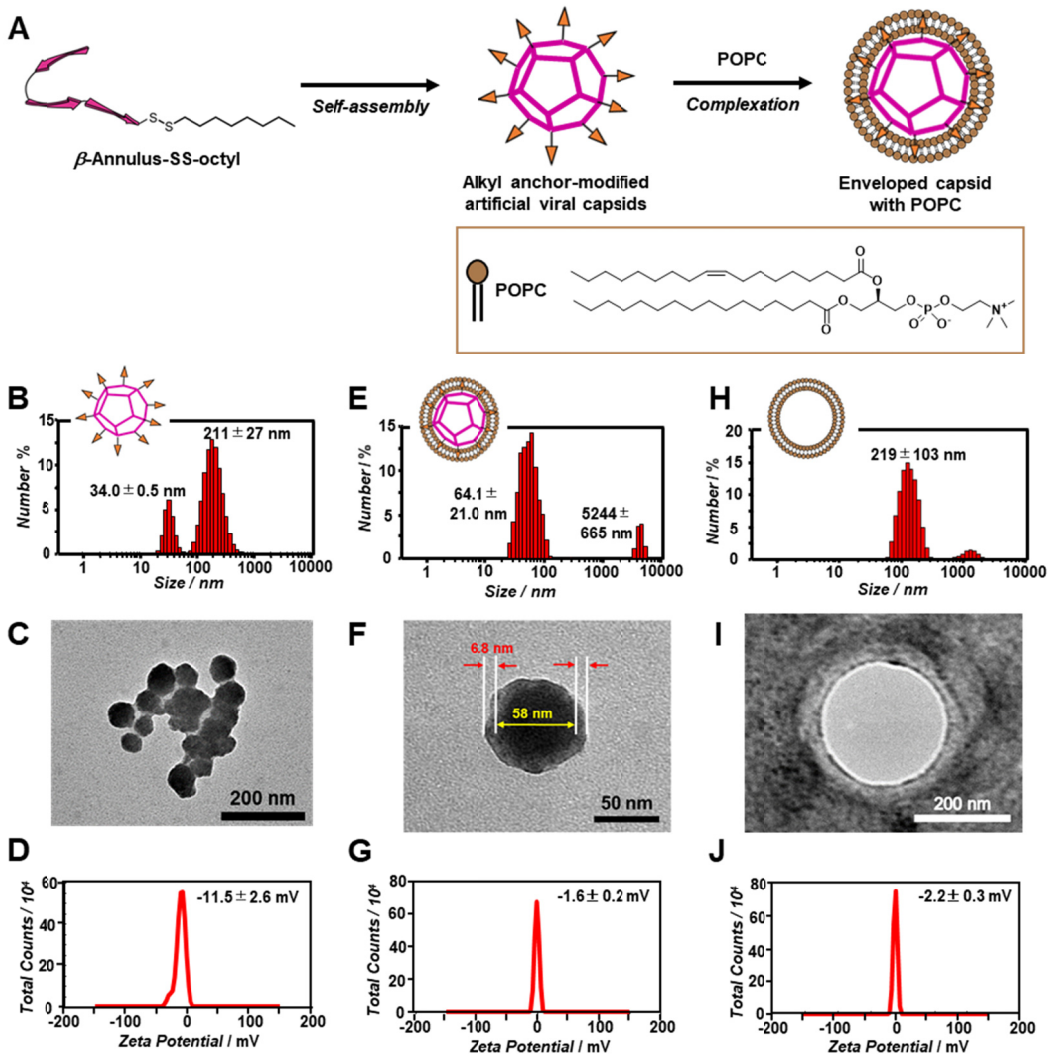

Figure 2. (A) Schematic illustration of the construction of the enveloped artificial viral capsid via hydrophobic interaction. (B–J) Size distributions obtained from DLS (B, E, H), TEM images (C, F, I), and ζ-potential (D, G, J) of the alkyl anchor-modified artificial viral capsid (B–D; 50 μM β-annulus–SS-octyl peptide), enveloped artificial viral capsid (E-G; 50 μM β-annulus–SS-octyl peptide, 5 mM POPC), and liposome (H-J; 5 mM POPC) in a 10 mM Tris-HCl buffer (pH 7.4, 5% DMSO) at 25ºC. The TEM samples were stained with an EM stainer.

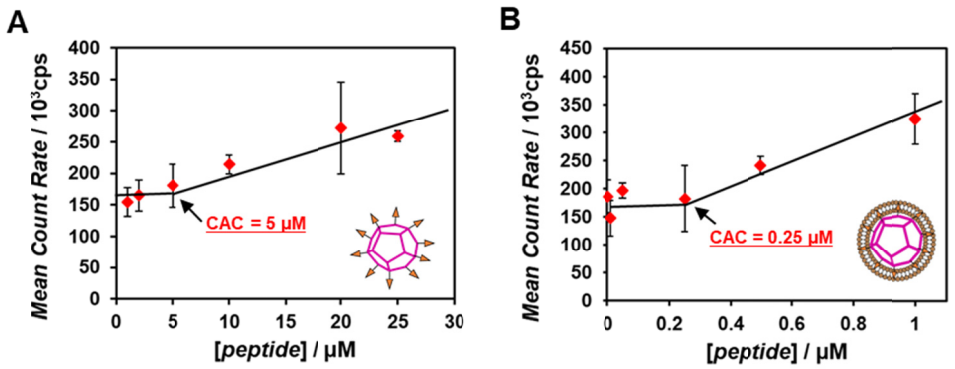

Figure 3. Concentration dependence of the β-annulus–SS-octyl peptide on the scattering intensity determined by DLS of alkyl anchor-modified artificial viral capsid (A) and enveloped artificial viral capsid (B) in a 10 mM Tris-HCl buffer (pH 7.4, 5% DMSO) at 25ºC.

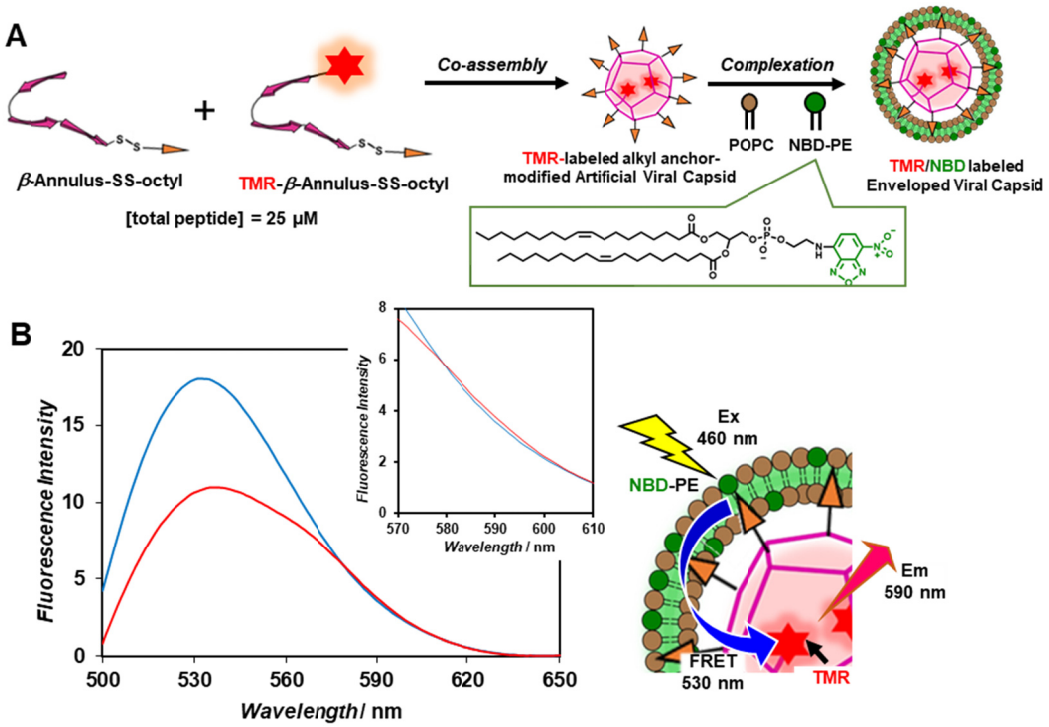

Figure 4. (A) Schematic illustration of the construction of the TMR/NBD-labeled enveloped artificial viral capsid. (B) Fluorescence emission spectra of the TMR/NBD-labeled enveloped artificial viral capsid comprising 10 μM NBD-PE, 4.99 mM POPC, 25 (blue) or 23.1 μM (red) β-annulus–SS-octyl peptide, and 0 (blue) or 1.9 μM (red) TMR–β-annulus-SS-octyl peptide excited at 460 nm in the 10 mM HEPES buffer (pH 7.4, 5% DMSO) at 25ºC. Schematic illustration of FRET between the TMR–β-annulus-SS-octyl peptide and NBD-PE on the enveloped artificial viral capsid.

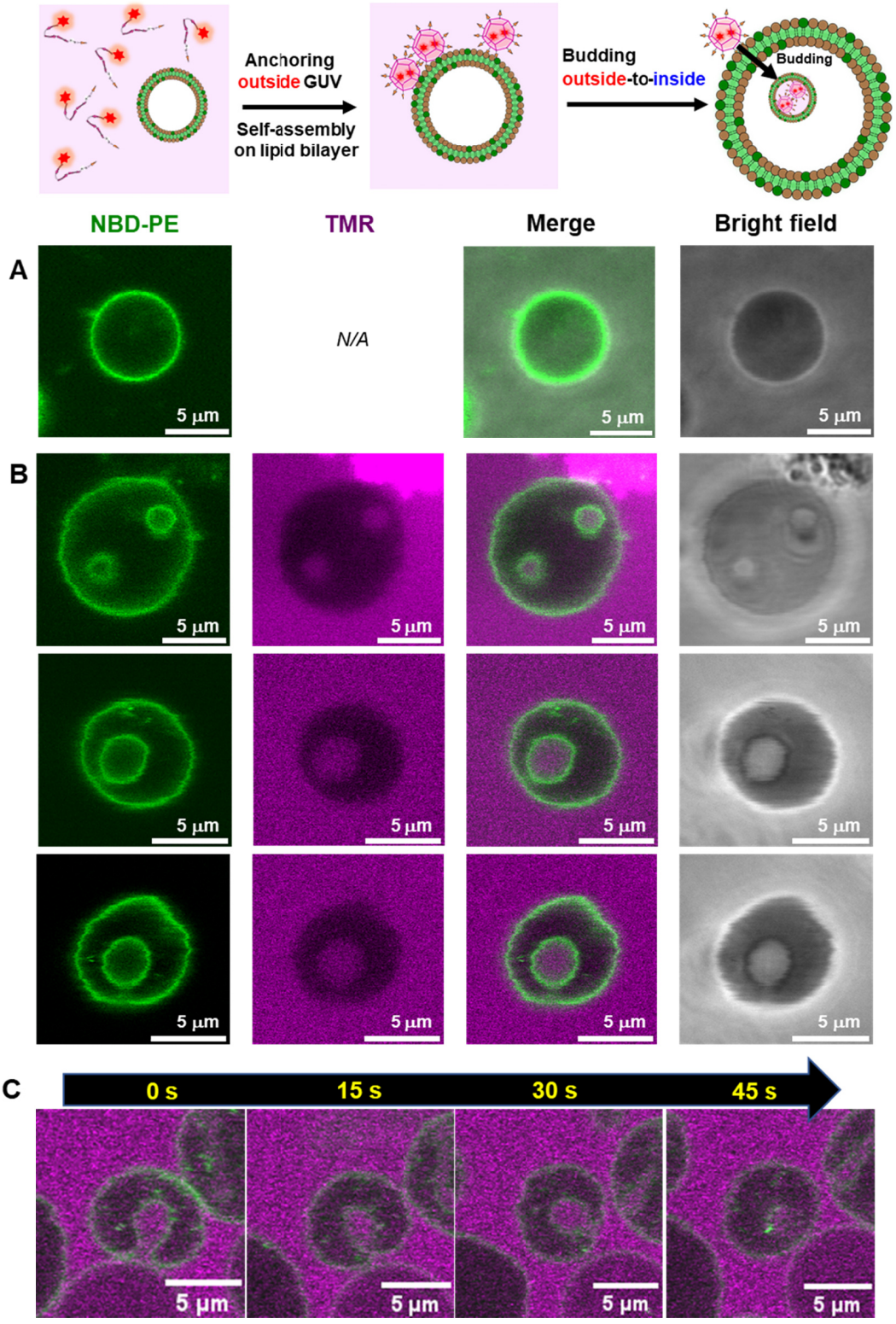

Figure 5. (A, B) CLSM images of the NBD-labeled POPC GUVs (1 mM POPC, 100 μM cholesterol, 10 μM NBD-PE) before (A) and after (B) adding 2 μM TMR–β-annulus–SS-octyl outside GUV. (C) Time-series CLSM images of NBD-labeled POPC GUV budding outside-to-inside. The elapsed time from the start of observation is shown. Channels for NBD-PE (green) and TMR (magenta), as well as bright fields of

the CLSM images. The inner aqueous phase of GUV comprised 150 mM sucrose and 350 mM glucose in a 10 mM HEPES buffer (pH 7.4), and the outer phase comprised 2 μM TMR–β-annulus–SS-octyl and 500 mM glucose in the 10 mM HEPES buffer containing 5% DMSO (pH 7.4).

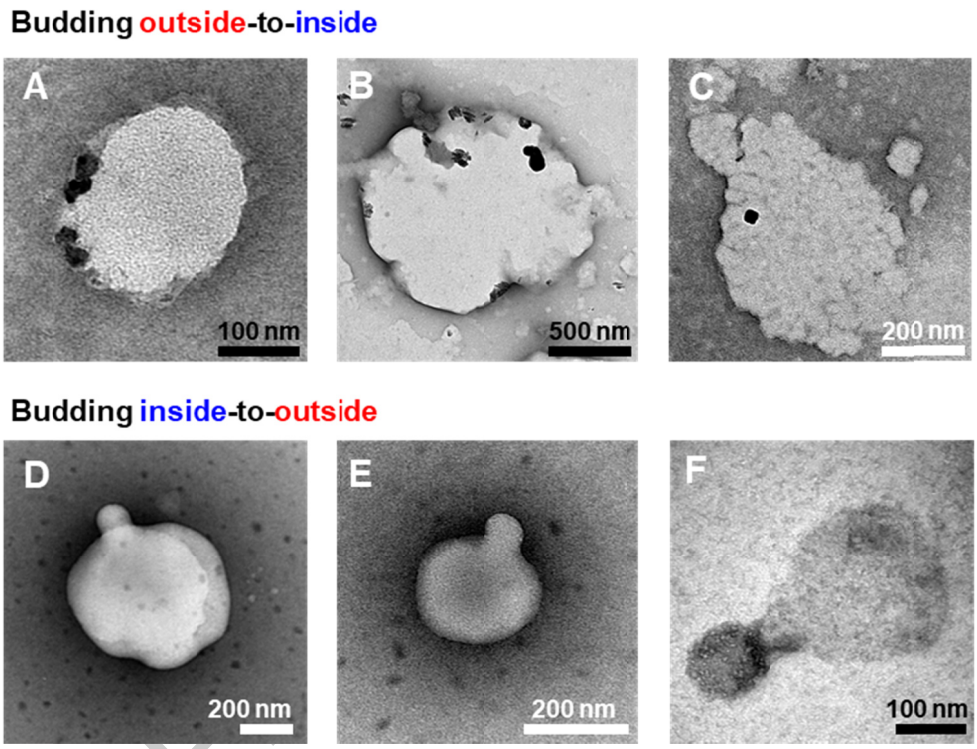

Figure 6. TEM images of the budding of POPC GUVs ([POPC] = 1 mM, [Cholesterol] = 100 μM, [NBD-PE] = 10 μM), following the addition of 2 μM TMR−β-annulus–SS-octyl outside (A-C) and inside (D-F) GUV. The TEM samples were stained with an EM stainer.

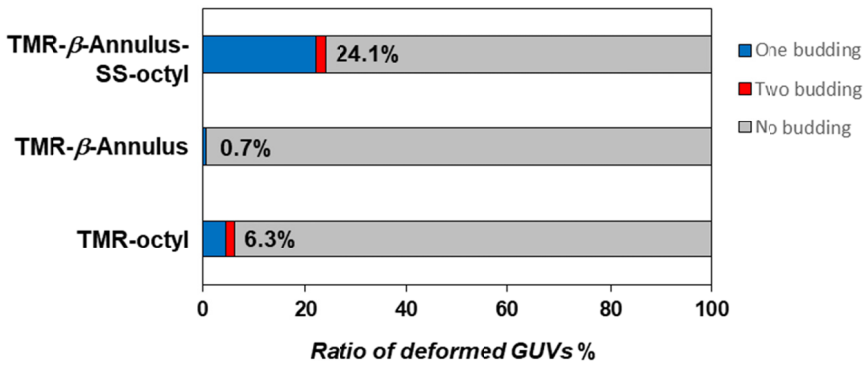

Figure 7. Ratio of the number of deformed POPC GUVs to the total number of POPC GUVs following the addition of 2 μM TMR–β-annulus–SS-octyl, TMR–β-annulus, or TMR–octyl outside (N >100).

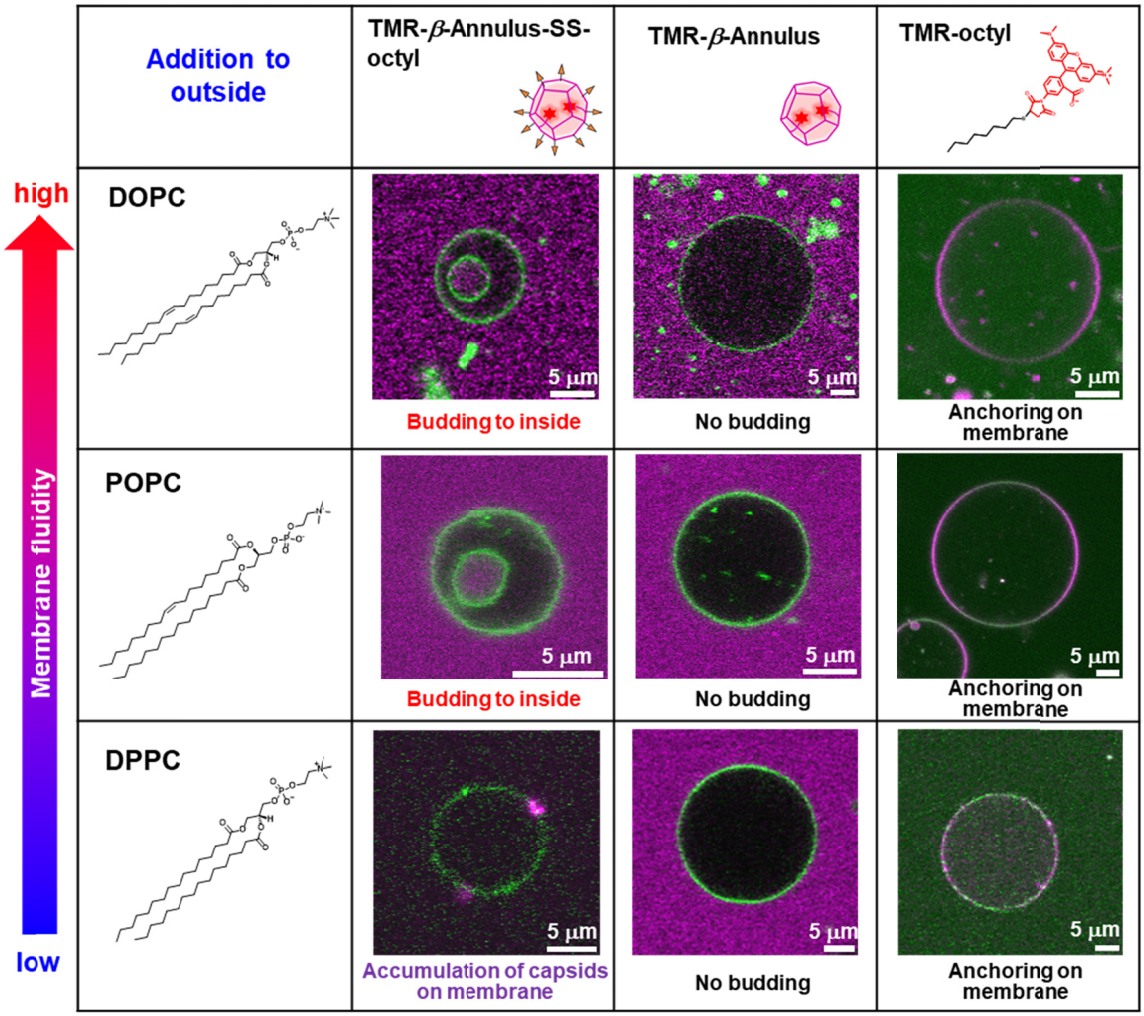

Figure 8. CLSM images of the NBD-labeled GUVs (DOPC, POPC, DPPC) with the addition of 2 μM TMR–β-annulus–SS-octyl, TMR–β-annulus, or TMR–octyl outside. Channels for NBD-PE (green) and TMR (magenta) of the CLSM images.

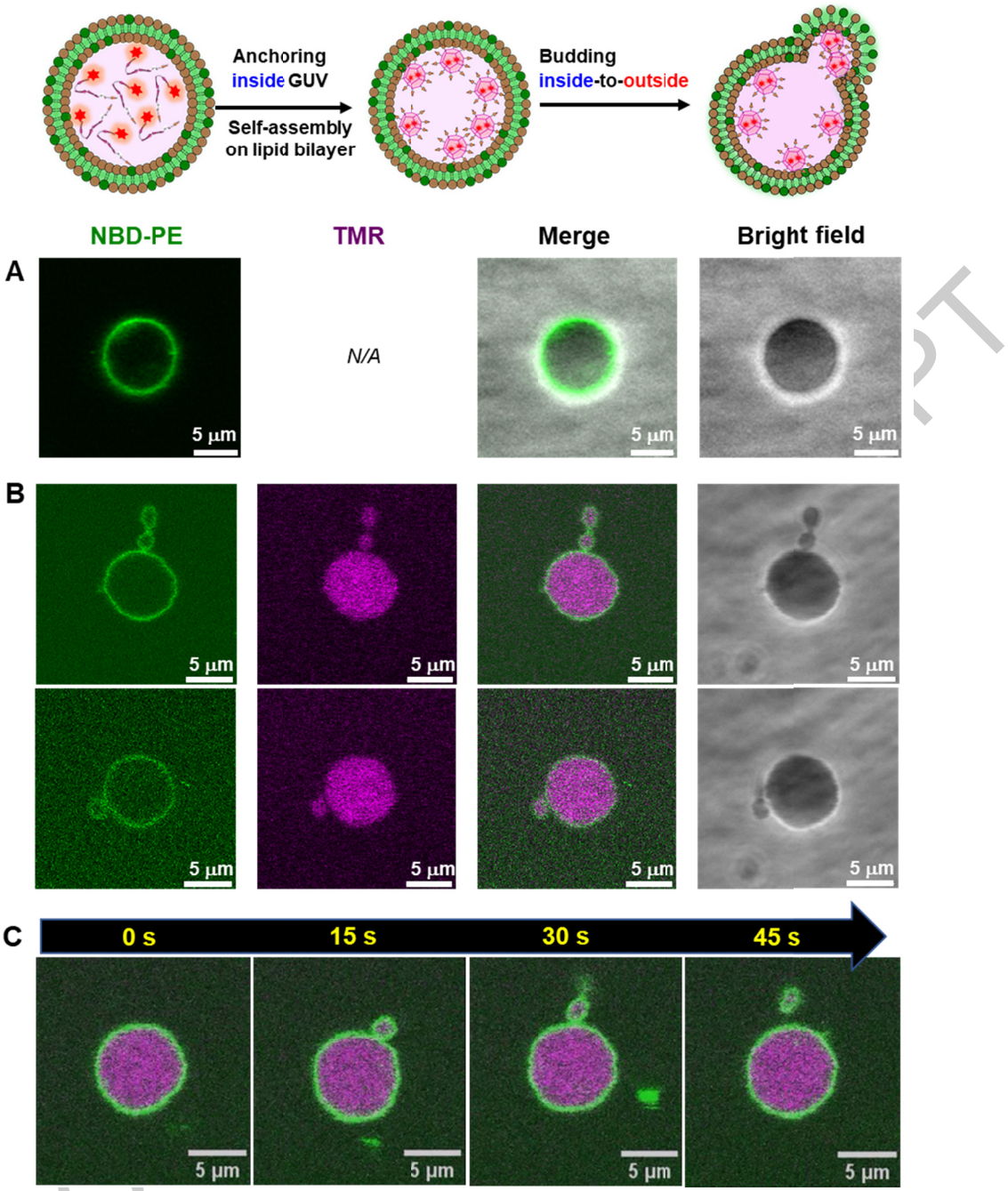

Figure 9. (A, B) CLSM images of NBD-labeled POPC GUVs (1 mM POPC, 100 μM cholesterol, 10 μM NBD-PE) before (A) and after (B) adding 2 μM TMR−β-annulus–SS-octyl inside GUV. (C) Time-series CLSM images of NBD-labeled POPC GUV budding inside-to-outside. The elapsed time from the start of observation is shown. Channels for NBD-PE (green) and TMR (magenta), as well as the bright field for the CLSM images. The inner aqueous phase of GUV comprises 2 μM TMR–β-annulus–SS-octyl, 150 mM sucrose, and 350 mM glucose in a 10 mM HEPES buffer containing 5%

DMSO (pH 7.4), and the outer phase comprises 500 mM glucose in the 10 mM HEPES buffer (pH 7.4).

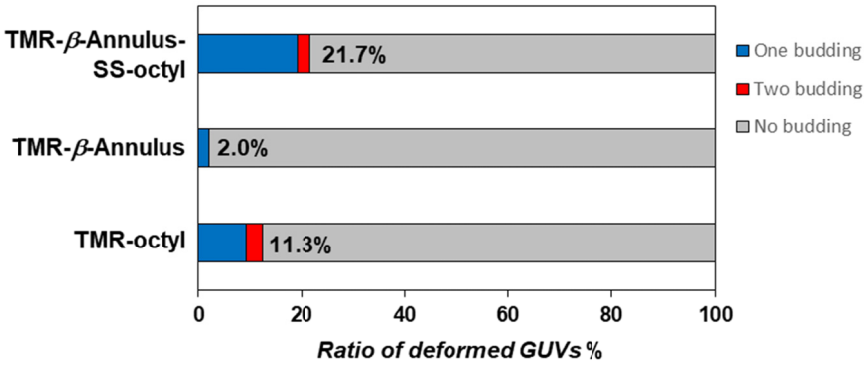

Figure 10. Ratio of the number of deformed POPC GUVs to the total number of POPC GUVs following the addition of 2 μM TMR–β-annulus–SS-octyl, TMR–β-annulus, or TMR–octyl inside (N >100).

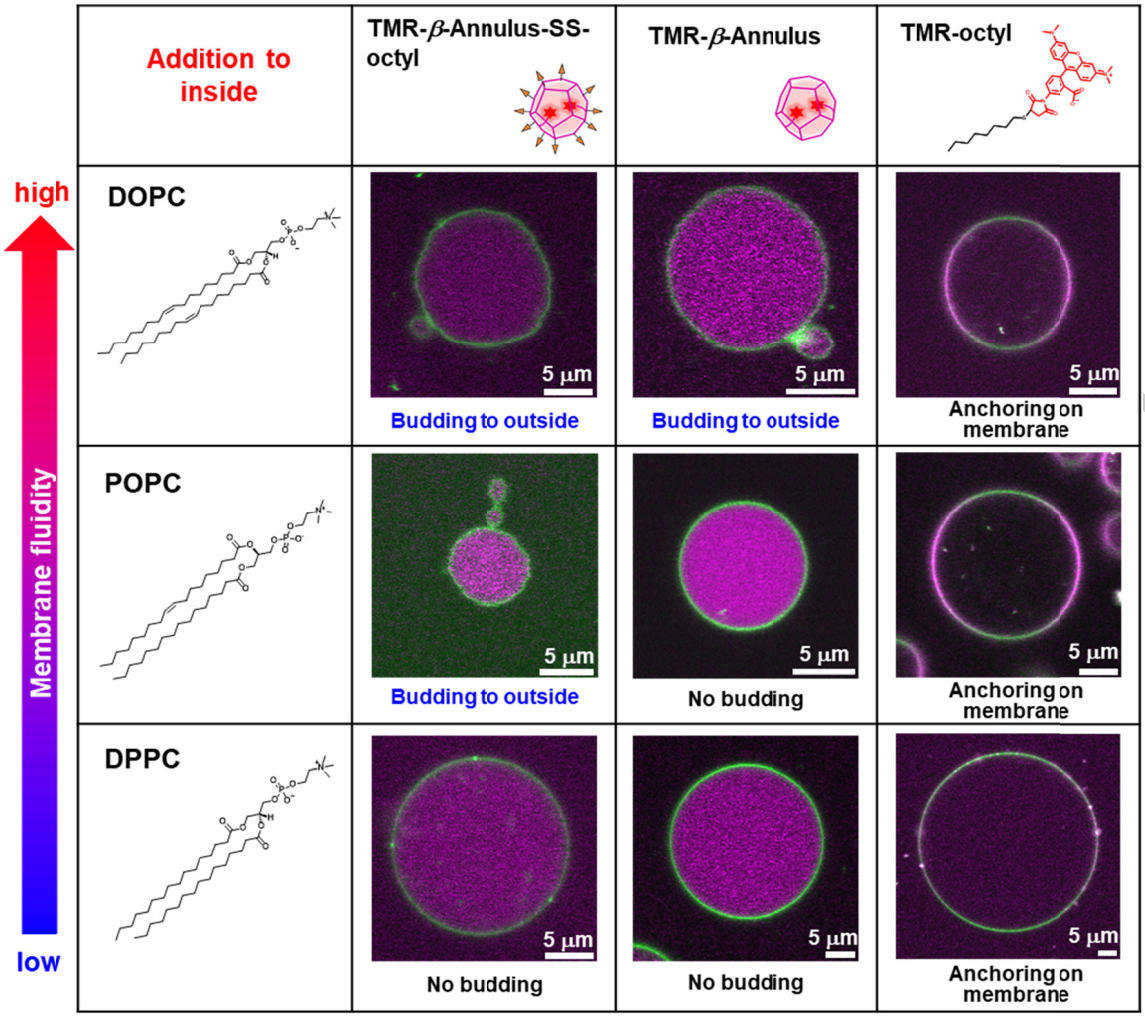

Figure 11. CLSM images of NBD-labeled GUVs (DOPC, POPC, **D**PPC) with the addition of 2 μM TMR–β-annulus–SS-octyl, TMR–β-annulus, or TMR–octyl inside. Channels for NBD-PE (green) and TMR (magenta) of the CLSM images.

Construction of an artificial viral budding system of GUVs using only synthesized molecules remains challenging. This study firstly demonstrate that budding outside-to-inside and inside-to-outside GUV were induced by addition of alkyl anchor-modified artificial viral capsid.

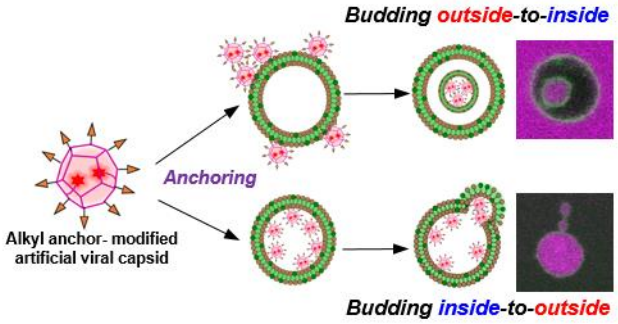

GA